[Research Paper] 대한금속 · 재료학회지 (*Korean J. Met. Mater.*), Vol. 61, No. 4 (2023) pp.269-276
DOI: 10.3365/KJMM.2023.61.4.269

Solid-State Synthesis and Thermoelectric Performance of $Cu_3Sb_{1-y}B^{III}_ySe_4$ (B^{III} = Al, In) Permingeatites

Ho-Jeong Kim and Il-Ho Kim*

Department of Materials Science and Engineering, Korea National University of Transportation, Chungju 27469, Republic of Korea

Abstract: Permingeatite (Cu_3SbSe_4) is a promising thermoelectric material with narrow bandgap energy and large carrier effective mass. However, doping is required to improve its electrical conductivity and thermoelectric properties. In this study, $Cu_3Sb_{1-y}(Al/In)_ySe_4$ doped with B^{III}-group elements (Al or In) at the Sb sites was synthesized using mechanical alloying followed by sintering through hot pressing. The resulting $Cu_3Sb_{1-y}(Al/In)_ySe_4$ contained a single phase of permingeatite with a tetragonal structure and therefore achieved a high relative density of 97.5–99.2%. The substitution of Al/In at the Sb sites produced lattice constants of a = 0.5652–0.5654 nm and c = 1.1249–1.1254 nm. As the Al/In doping content increased, the carrier (hole) concentration increased, reducing the Seebeck coefficient and increasing the electrical and thermal conductivities. Substituting Al^{3+} or In^{3+} at the Sb^{5+} site can generate additional carriers, resulting in a high electrical conductivity of (1.4–1.1) × 10^4 Sm^{-1} at 323–623 K for $Cu_3Sb_{0.92}In_{0.08}Se_4$. $Cu_3Sb_{0.96}Al_{0.04}Se_4$ exhibited a maximum power factor of 0.51 $mWm^{-1}K^{-2}$ at 623 K and a minimum thermal conductivity of 0.74 $Wm^{-1}K^{-1}$, resulting in a maximum dimensionless figure of merit, ZT, of 0.42 at 623 K. $Cu_3Sb_{0.96}In_{0.04}Se_4$ obtains a ZT of 0.47 at 623 K, indicating a high power factor of 0.65 $mWm^{-1}K^{-2}$ at 623 K and low thermal conductivity of 0.84 $Wm^{-1}K^{-1}$ at 523 K.

(Received 31 October, 2022; Accepted 3 January, 2023)

Keywords: thermoelectric, permingeatite, mechanical alloying, hot pressing, doping

1. INTRODUCTION

Thermoelectric materials and devices have attracted much interest because they provide eco-friendly and economical energy-conversion [1,2]. Thermoelectric materials can be employed in energy-harvesting technologies to directly convert waste heat into electricity [3]. The thermoelectric energy-conversion efficiency (η) is defined as

$$\eta = \frac{T_H - T_C}{T_H} \cdot \frac{\sqrt{1+ZT_M}-1}{\sqrt{1+ZT_M}+\frac{T_C}{T_H}} \quad (1)$$

where T_H is the temperature of the hot junction, T_C is the temperature of the cold junction, and T_M is the average of T_H and T_C. In Eq. 1, the first term is the Carnot efficiency, the second term is the material efficiency, and ZT is a dimensionless figure of merit given by

$$ZT = \frac{\alpha^2 \sigma}{\kappa} T \quad (2)$$

ZT depends on the Seebeck coefficient (α), electrical conductivity (σ), thermal conductivity (κ), and absolute temperature (T) [1,3]. Therefore, to improve the energy-conversion efficiency, the material efficiency must be increased (high ZT) along with the Carnot efficiency (application at high temperatures). Increasing the ZT value requires maximizing the power factor ($\alpha^2\sigma$) while minimizing the thermal conductivity. However, it is difficult to optimize these simultaneously because the Seebeck coefficient, electrical conductivity, and thermal conductivity are all affected by the carrier concentration [4].

Permingeatite, a Cu-Sb-Se chalcogenide (Cu_3SbSe_4), belongs to the space group $I\bar{4}2m$ derived from the zinc-blende structure [5-8]. Its crystal structure consists of $CuSe_4$ tetrahedra with three-dimensional frameworks of Cu–Se bonds and $SbSe_4$ tetrahedra with one-dimensional Sb–Se

- 김호정: 학사과정, 김일호: 교수
*Corresponding Author: Il-Ho Kim
[Tel: +82-10-5338-1582, E-mail: ihkim@ut.ac.kr]

bonds [6,8]. Because the Sb–Se bond is longer than the Cu–Se bond, the anisotropy in the charge transport and phonon scattering increases, affecting electrical and thermal properties [3,8]. Cu_3SbSe_4 is attracting attention because of its narrow band gap and high carrier effective mass; however, it has the disadvantages of low carrier concentration (low electrical conductivity) and high thermal conductivity [1,5].

By partially substituting other elements into Cu_3SbSe_4, its thermoelectric performance can be improved by optimizing the carrier concentration and reducing the lattice thermal conductivity, resulting in a higher power factor, because of phonon scattering. Studies are underway to improve thermoelectric performance further by replacing group 14 (B^{IV}) elements at the group 15 (B^{V}) Sb sites. Wei et al. [9] reported a maximum ZT of 0.7 at 673 K for $Cu_3Sb_{0.98}Sn_{0.02}Se_4$ prepared by mechanical alloying (MA) and spark plasma sintering (SPS). Chang et al. [10] obtained a maximum ZT of 0.70 at 640 K for $Cu_{2.95}Sb_{0.96}Ge_{0.04}Se_4$ synthesized using the melting-quenching-annealing and SPS processes. Pi et al. [11] achieved a maximum ZT of 0.65 at 623 K for $Cu_3Sb_{0.86}Ge_{0.14}Se_4$, prepared through MA, followed by hot pressing (HP). García et al. [6] predicted that As could lead to the highest ZT value at 300 K, among $Cu_3Sb_{1-x}M_xSe_4$ (M = Al, Ga, In, Tl, Si, Ge, Sn, Pb, As, Bi; decreasing in the order of Bi, P, Si, Ge, Pb, Sn, In, Tl, Ga, and Al), using the density-functional theory and Boltzmann semiclassical transport theory. Studies on doping group 13 (B^{III}) element at the Sb sites have also been reported. Zhao et al. [12] obtained a maximum ZT of 0.54 at 650 K for $Cu_3Sb_{0.985}Ga_{0.015}Se_4$ prepared by melting, annealing, and SPS. Li et al. [13] reported a maximum ZT of 0.58 at 600 K for $Cu_3Sb_{0.97}Al_{0.03}Se_4$ synthesized by melting-quenching-annealing and SPS. Zhang et al. [14] achieved a maximum ZT of 0.50 at 648 K for $Cu_3Sb_{0.997}In_{0.003}Se_4$ produced by melting-quenching-annealing and HP.

In this study, $Cu_3Sb_{1-y}Al_ySe_4$ (y = 0.02–0.08) and $Cu_3Sb_{1-y}In_ySe_4$ (y = 0.02–0.08) were prepared by the MA-HP method using solid-state and dry processes, respectively. The phase, charge transport, and thermoelectric properties were examined. Al^{3+} and In^{3+} have two fewer valence electrons than Sb^{5+}, and thus, good acceptor roles can be expected in Cu_3SbSe_4.

2. EXPERIMENTAL PROCEDURE

Al and In-doped permingeatites $Cu_3Sb_{1-y}Al_ySe_4$ (y = 0.02, 0.04, 0.06, and 0.08) and $Cu_3Sb_{1-y}In_ySe_4$ (y = 0.02, 0.04, 0.06, and 0.08) were produced using elemental powders of Cu (purity 99.9%, < 45 μm, Kojundo), Sb (purity 99.999%, < 150 μm, Kojundo), Se (purity 99.9%, < 10 μm, Kojundo), Al (purity 99.9%, < 106 μm, Kojundo), and In (purity 99.99%, < 75 μm, Kojundo). A mixed powder (20 g) corresponding to the stoichiometric composition and stainless steel balls of diameter 5 mm (400 g) were placed in a hardened steel jar and mechanically alloyed at 350 rpm for 12 h in Ar atmosphere. The synthesized Al/In-doped permingeatite powders were hot-pressed at 573 K for 2 h under 70 MPa in vacuum using a graphite mold with an inner diameter of 10 mm.

X-ray diffraction (XRD; Bruker, D8-Advance) using Cu Kα radiation (40 kV, 30 mA) was performed to analyze the phases, crystallographic information, and lattice parameters. The hot-pressed samples were cut into disks of 1 mm (thickness) × 10 mm (diameter) for XRD analysis. 2θ diffraction angles of 10–90° were measured at a scanning step of 0.02°. Rietveld refinement (TOPAS program) was used to calculate the lattice constants. Using scanning electron microscopy (SEM; FEI, Quanta400), the microstructures of the hot-pressed specimens were observed in the backscattered electron (BSE) mode, and the elemental line scans and maps were analyzed according to the energy level of each element using an energy-dispersive spectrometer (EDS; Bruker, XFlash4010). The Hall coefficient was measured using the van der Pauw method (Keithley 7065) under a magnetic field of 1 T and an electric current of 100 mA to evaluate the carrier type, concentration, and mobility. The specimen was cut into rectangular columns of 3 mm × 3 mm × 9 mm to measure the Seebeck coefficient and electrical conductivity using ZEM-3 equipment (Ulvac-Riko) in He atmosphere. The specimen was also cut into a disk shape of 1 mm (thickness) × 10 mm (diameter) to measure thermal diffusivity, specific heat, and density, using a TC-9000H (Ulvac-Riko) system in vacuum. The temperature dependence of the thermoelectric properties was examined in the temperature range of 323–623 K, and the power factor and dimensionless figure of merit were evaluated.

3. RESULTS AND DISCUSSION

Figure 1 shows the XRD patterns of the $Cu_3Sb_{1-y}B^{III}{}_ySe_4$ powders synthesized by MA. The diffraction peaks of all the specimens indicate a single permingeatite phase with a tetragonal structure, which is consistent with the standard diffraction pattern (ICDD PDF# 01-085-0003) of permingeatite. This confirmed that the solid-state synthesis of Al/In-doped permingeatite compounds is possible using MA.

Figure 2 presents the XRD patterns of $Cu_3Sb_{1-y}B^{III}{}_ySe_4$ sintered by HP. The tetragonal permingeatite phase remained after HP at 573 K, and no phase changes or secondary phases were detected. Rietveld analysis was conducted to determine changes in the lattice constants, due to the Al and In doping (substitution). The calculated lattice constants are listed in Table 1. The Al doping changes the a-axis from 0.5649 to 0.5652–0.5653 nm and the c-axis from 1.1247 to 1.1249–1.1251 nm. The In doping increases the a-axis to 0.5653–0.5654 nm and the c-axis to 1.1253–1.1254 nm. This indicates that, although Al and In were successfully substituted at the Sb sites, the changes in the lattice constants with the change in doping content are not significant. Shannon [15] reported the ionic radii of Sb^{5+} (62 pm), Al^{3+} (30 pm), and In^{3+} (80 pm). Considering the electronegativities of Sb (2.05), Al (1.61), and In (1.78), reported by Allred [16], In can be expected to replace Sb more easily than Al. Li et al. [13] reported that Al doping of $Cu_3Sb_{1-x}Al_xSe_4$ (x = 0–0.03) reduced the lattice constants from 0.5654 to 0.5601–0.5635 nm on the a-axis and from 1.1196 to 1.1137–1.1175 nm on the c-axis. However, Ghanwat et al. [17,18] reported

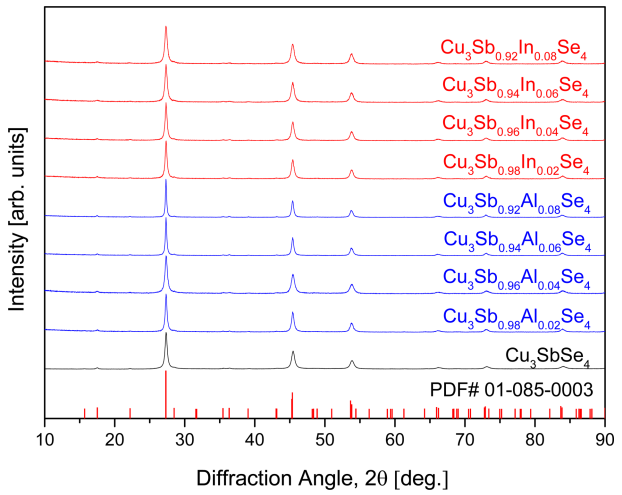

Fig. 1. XRD patterns of mechanically alloyed $Cu_3Sb_{1-y}(Al/In)_ySe_4$.

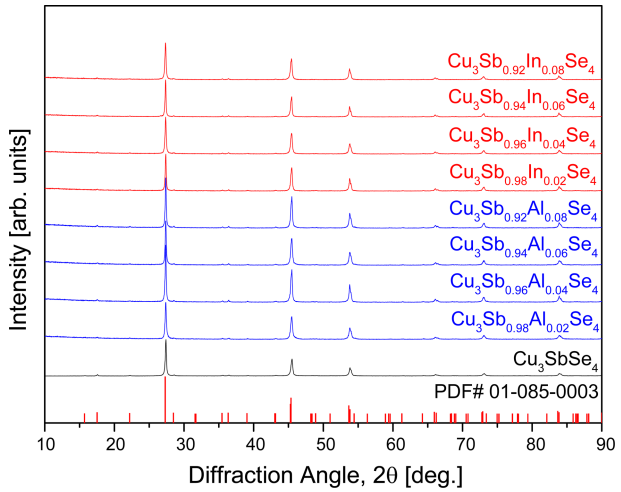

Fig. 2. XRD patterns of hot-pressed $Cu_3Sb_{1-y}(Al/In)_ySe_4$.

Table 1. Relative density, lattice constant, and Lorenz number of $Cu_3Sb_{1-y}(Al/In)_ySe_4$.

Specimen	Relative Density [%]	Lattice Constant [nm]		Lorenz Number [10^{-8} V^2K^{-2}]
		a-axis	c-axis	
Cu_3SbSe_4	98.1	0.5649	1.1247	1.5712
$Cu_3Sb_{0.98}Al_{0.02}Se_4$	98.0	0.5653	1.1250	1.8150
$Cu_3Sb_{0.96}Al_{0.04}Se_4$	97.6	0.5652	1.1249	1.5773
$Cu_3Sb_{0.94}Al_{0.06}Se_4$	97.5	0.5653	1.1250	1.7628
$Cu_3Sb_{0.92}Al_{0.08}Se_4$	97.8	0.5653	1.1251	1.7697
$Cu_3Sb_{0.98}In_{0.02}Se_4$	99.2	0.5654	1.1253	1.2003
$Cu_3Sb_{0.96}In_{0.04}Se_4$	98.8	0.5653	1.1253	1.7107
$Cu_3Sb_{0.94}In_{0.06}Se_4$	98.2	0.5653	1.1253	1.7428
$Cu_3Sb_{0.92}In_{0.08}Se_4$	98.6	0.5653	1.1254	1.7757

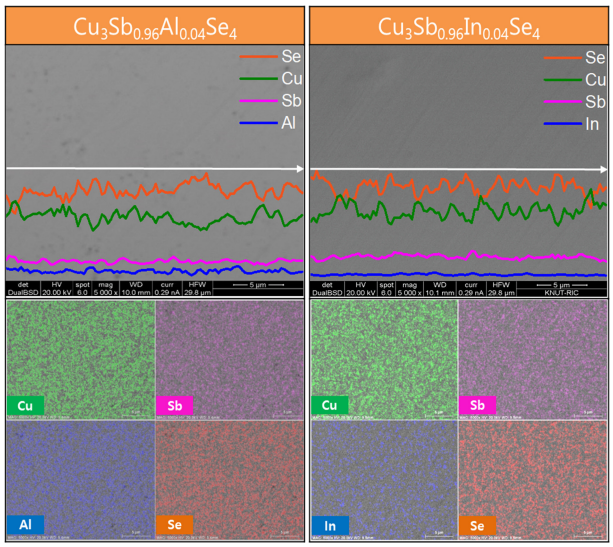

Fig. 3. BSE-SEM images with EDS line scans and elemental maps of $Cu_3Sb_{0.96}(Al/In)_{0.04}Se_4$.

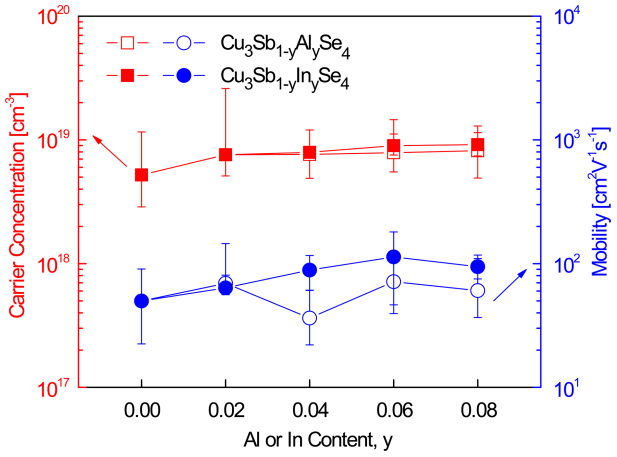

Fig. 4. Charge-transport properties of $Cu_3Sb_{1-y}(Al/In)_ySe_4$.

that the doping of In in $Cu_3Sb_{1-x}In_xSe_4$ (x = 0.02–0.10) increased the lattice constants from 0.56603 to 0.56607–0.56636 nm on the a-axis and from 1.12843 to 1.12848–1.12876 nm on the c-axis.

Figure 3 shows the BSE-SEM images and EDS elemental line scans and maps of $Cu_3Sb_{0.96}B^{III}_{0.04}Se_4$. A dense microstructure without pores or cracks was observed, with a high relative density (sintered) (Table 1). No secondary phases were observed, which is consistent with the XRD phase analysis results (Figure 2). The EDS elemental analysis confirmed that all elements were uniformly distributed.

Figure 4 shows the charge-transport properties of $Cu_3Sb_{1-y}B^{III}_ySe_4$. Both the undoped and Al/In-doped specimens exhibited p-type conduction characteristics with holes as the majority carriers, representing positive Hall coefficients. The undoped Cu_3SbSe_4 had a carrier concentration of 5.2×10^{18} cm^{-3} and mobility of 49.9 $cm^2V^{-1}s^{-1}$. As the doping content of Al and In increased, the carrier concentration tended to increase (8.2×10^{18} cm^{-3} for the Al-doped permingeatite and 9.2×10^{18} cm^{-3} for the In-doped permingeatite when y = 0.08). Li et al. [13] reported a carrier concentration of 8.04×10^{17} cm^{-3} and mobility of 94.1 $cm^2V^{-1}s^{-1}$ for Cu_3SbSe_4. The carrier concentration increased and mobility decreased for $Cu_3Sb_{1-y}Al_ySe_4$ upon increasing the Al doping content; when y = 0.03, the carrier concentration was 1.19×10^{19} cm^{-3} and mobility was 52.5 $cm^2V^{-1}s^{-1}$. Zhang et al. [14] reported that the carrier concentration of 2.2×10^{18} cm^{-3} (mobility of 65 $cm^2V^{-1}s^{-1}$) for Cu_3SbSe_4 increased by increasing the In doping level in $Cu_3Sb_{1-y}In_ySe_4$ (reached 3.5×10^{19} cm^{-3} when y = 0.004). Brooks [19] suggested that, theoretically, an increase in the carrier concentration could reduce mobility in a nondegenerate semiconductor. However, in this study, the mobility increased slightly as the carrier concentration increased. This was believed to be due to the transition from the nondegenerate state to the degenerate state, following Al and In doping. Suzumura et al. [20] reported that both the carrier concentration and mobility could be increased by doping, in degenerate semiconductors.

Figure 5 shows the temperature dependence of the electrical conductivity of $Cu_3Sb_{1-y}B^{III}_ySe_4$. In undoped and Al-doped permingeatites, the electrical conductivity increases slightly when increasing the temperature. However, In-doped permingeatites exhibit degenerate semiconductor behavior with little temperature dependence. At a certain temperature, the electrical conductivity increased with increasing Al and In content. The In-doped specimens exhibited higher electrical conductivities than the Al-doped ones, because their carrier concentrations and mobilities were higher, as shown in Figure 4. Replacing Al^{3+} or In^{3+} at the Sb^{5+} site of Cu_3SbSe_4 can generate additional carriers (holes), resulting in an increase in electrical conductivity. The highest electrical conductivity of $(1.4–1.1) \times 10^4$ Sm^{-1} was obtained at 323–623 K for $Cu_3Sb_{0.92}In_{0.08}Se_4$. Li et al. [13] reported that the electrical conductivity increased upon increasing the Al

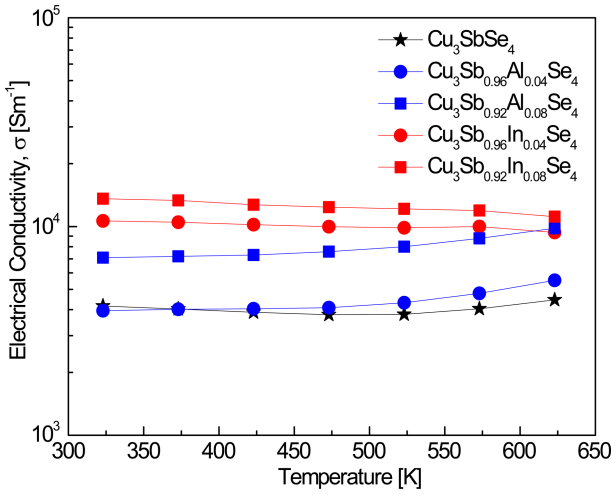

Fig. 5. Temperature dependence of the electrical conductivity of $Cu_3Sb_{1-y}(Al/In)_ySe_4$.

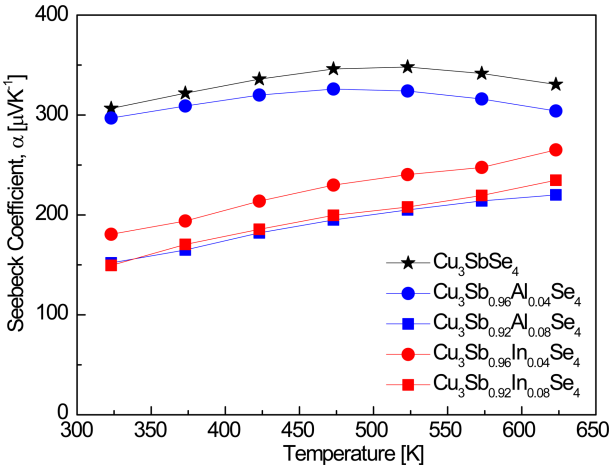

Fig. 6. Temperature dependence of the Seebeck coefficient of $Cu_3Sb_{1-y}(Al/In)_ySe_4$.

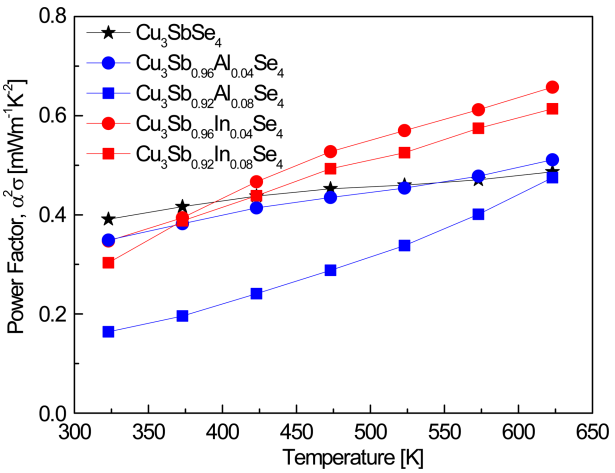

Fig. 7. Temperature dependence of the power factor of $Cu_3Sb_{1-y}(Al/In)_ySe_4$.

content in $Cu_3Sb_{1-y}Al_ySe_4$. The highest electrical conductivity of (0.5–0.7) × 10^4 Sm^{-1} was attained at 300–600 K for $Cu_3Sb_{0.97}Al_{0.03}Se_4$. Zhang et al. [14] obtained the highest electrical conductivity of (1.0–1.8) × 10^4 Sm^{-1} at 300–650 K for $Cu_3Sb_{0.996}In_{0.004}Se_4$.

Figure 6 presents the temperature dependence of the Seebeck coefficient of $Cu_3Sb_{1-y}B^{III}_ySe_4$. All positive Seebeck coefficient values confirm that the majority carriers are holes in p-type semiconductors [7]. At a certain temperature, as the Al and In doping contents increase, the carrier concentration increases, and thus, the Seebeck coefficient decreases. In addition, the Seebeck coefficient increases as the temperature increases. However, for Cu_3SbSe_4 and $Cu_3Sb_{0.96}Al_{0.04}Se_4$ it decreased at temperatures above 500 K because of the intrinsic transition. The Seebeck coefficient of $Cu_3Sb_{0.96}Al_{0.04}Se_4$ decreased to 326 μVK^{-1} at 623 K after reaching a maximum value of 304 μVK^{-1} at 473 K as the temperature increased.

The reason for the decrease in the Seebeck coefficient above a certain temperature is the increase in the concentration of electrons, which are minority carriers that are thermally activated from the valence band. Li et al. [13] explained that the Seebeck coefficient decreased as the Al content increased in $Cu_3Sb_{1-y}Al_ySe_4$, and as the temperature increased, the Seebeck coefficient gradually decreased for y = 0.01 and 0.02, but increased for y = 0.03. This is the characteristic of a degenerate semiconductor. The Seebeck coefficient was 150–225 μVK^{-1} at 300–600 K for $Cu_3Sb_{0.97}Al_{0.03}Se_4$. Zhang et al. [14] reported that for $Cu_3Sb_{1-y}In_ySe_4$the Seebeck coefficient decreased by increasing the In content, and it increased as the temperature increased and then decreased at temperatures above 475 K, indicating a degenerate semiconductor behavior. $Cu_3Sb_{0.997}In_{0.003}Se_4$ exhibited 230–290 μVK^{-1} at 300–650 K.

Figure 7 shows the temperature dependence of the power factor of $Cu_3Sb_{1-y}B^{III}_ySe_4$. The power factor is an index related to the electrical output power of a thermoelectric device (power generator), which is proportional to the Seebeck coefficient and electrical conductivity [1]. The power factor of Cu_3SbSe_4 was as low as 0.39–0.49 $mWm^{-1}K^{-2}$ at 323–623 K and had a small temperature

dependence. As a result of doping with Al or In, the power factor increased rapidly as the temperature increased. In particular, for the In-doped specimens, the power factor improved at high temperatures. At 623 K, Cu_3SbSe_4 exhibited a power factor of 0.49 $mWm^{-1}K^{-2}$ and $Cu_3Sb_{0.96}Al_{0.04}Se_4$ exhibited a power factor of 0.51 $mWm^{-1}K^{-2}$, while $Cu_3Sb_{0.96}In_{0.04}Se_4$ exhibited the highest power factor of 0.66 $mWm^{-1}K^{-2}$. Li et al. [13] reported that all $Cu_3Sb_{1-y}Al_ySe_4$ had higher power factor values than Cu_3SbSe_4, and that $Cu_3Sb_{0.97}Al_{0.03}Se_4$ achieved a very high power factor of 1.05 $mWm^{1}K^{-2}$ at 600 K. Zhang et al. [14] reported that $Cu_3Sb_{1-y}In_ySe_4$ exhibited higher power factor values than Cu_3SbSe_4 at temperatures above 400 K, and a maximum power factor of 0.75 $mWm^{-1}K^{-2}$ at 648 K was achieved for $Cu_3Sb_{0.998}In_{0.002}Se_4$.

Figure 8 shows the thermal conductivity, lattice thermal conductivity, and electronic thermal conductivity of $Cu_3Sb_{1-y}B^{III}_ySe_4$. The thermal conductivity is determined by the heat transfer by both phonons and charge carriers [21,22]. As shown in Figure 8 (a), the thermal conductivity decreased as the temperature increased. $Cu_3Sb_{0.96}Al_{0.04}Se_4$ had the lowest thermal conductivity of 0.74 $Wm^{-1}K^{-1}$ at 623 K, and $Cu_3Sb_{0.96}In_{0.04}Se_4$ had the lowest thermal conductivity of 0.84 $Wm^{-1}K^{-1}$ at 523 K. However, the thermal conductivity increased as the Al and In doping contents increased at a constant temperature. Li et al. [13] reported that the thermal conductivity of $Cu_3Sb_{1-y}Al_ySe_4$ decreased with increasing temperature from 300 to 600 K, and was greater than that of Cu_3SbSe_4 at a constant temperature. $Cu_3Sb_{0.97}Al_{0.03}Se_4$ exhibited a minimum thermal conductivity of 1.1 $Wm^{-1}K^{-1}$ at 600 K. Zhang et al. [14] reported that the thermal conductivity of $Cu_3Sb_{1-y}In_ySe_4$ decreased with increasing temperature from 300 to 650 K, which was related to a decrease in lattice thermal conductivity because of the increase in point defect scattering. $Cu_3Sb_{0.997}In_{0.003}Se_4$ had a minimum thermal conductivity of 0.5 $Wm^{-1}K^{-1}$ at 648 K.

Figure 8 (b) shows the lattice thermal conductivity (κ_L). The thermal conductivity of permingeatite is dominantly dependent on the lattice thermal conductivity. The reduction in lattice thermal conductivity by the substitution of Al or In at the Sb sites was not significant. Cu_3SbSe_4 exhibited κ_L values of 1.17–0.72 $Wm^{-1}K^{-1}$ at 323–623 K. Minimum κ_L values of 0.69 and 0.76 $Wm^{-1}K^{-1}$ were achieved at 523 K for

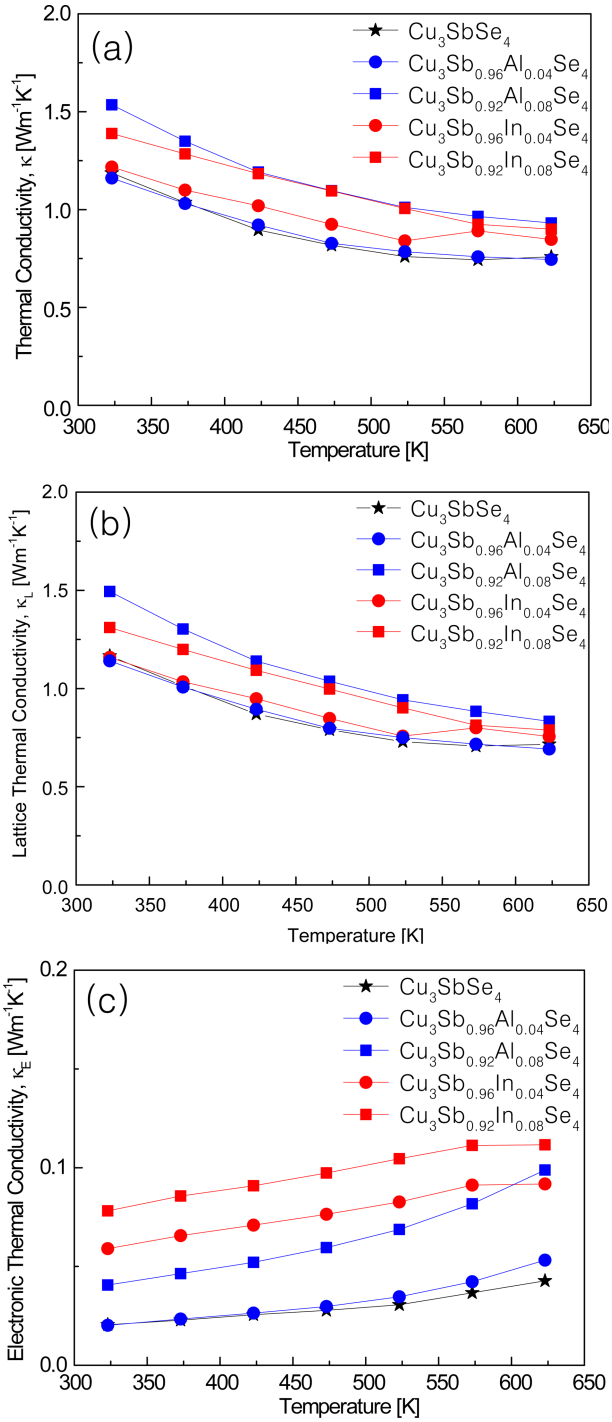

Fig. 8. Temperature dependence of the thermal conductivity of $Cu_3Sb_{1-y}(Al/In)_ySe_4$: (a) total thermal conductivity, (b) lattice thermal conductivity, and (c) electronic thermal conductivity.

$Cu_3Sb_{0.96}Al_{0.04}Se_4$ and $Cu_3Sb_{0.96}In_{0.04}Se_4$, respectively. Li et al. [13] estimated the lattice thermal conductivity by subtracting the carrier thermal conductivity from the total

thermal conductivity, which was calculated by the Wiedemann–Franz law; at 600 K, $Cu_3Sb_{0.97}Al_{0.03}Se_4$ had a maximum carrier thermal conductivity of 0.25 $Wm^{-1}K^{-1}$ with a minimum κ_L of 0.8 $Wm^{-1}K^{-1}$. Zhang et al. [14] reported that the lattice thermal conductivity of $Cu_3Sb_{1-y}In_ySe_4$ (y = 0.002–0.004) decreased with T^{-1} in the temperature range of 300–650 K, indicating that the Umklapp (phonon–phonon) scattering was dominant in the phonon transport. Using Cahill's formula, the lowest κ_L of $Cu_3Sb_{0.997}In_{0.003}Se_4$ was estimated to be 0.8 $Wm^{-1}K^{-1}$ at 650 K.

Figure 8(c) shows the electronic thermal conductivity (κ_E), which can be expressed using the Wiedemann–Franz law (Eq. 3):

$$\kappa_E = L\sigma T \quad (3)$$

where L is the temperature-dependent Lorenz number [7,8]. The Lorenz numbers used in the study are listed in Table, which were calculated using the formula [23]:

$$L = 1.5 + exp(-|\alpha|/116) \quad (4)$$

Although κ_L shows a negative temperature dependence, κ_E shows a positive temperature dependence. The κ_E of Cu_3SbSe_4 was 0.02–0.04 $Wm^{-1}K^{-1}$ at 323–623 K. However, because the carrier concentration is increased by Al and In doping, $Cu_3Sb_{0.92}Al_{0.08}Se_4$ and $Cu_3Sb_{0.92}In_{0.08}Se_4$ exhibited higher κ_E values of 0.09 and 0.11 $Wm^{-1}K^{-1}$, respectively, at 623 K.

Figure 9 shows the ZT values of $Cu_3Sb_{1-y}B^{III}{}_ySe_4$. The ZT values increased with increasing temperature, and Cu_3SbSe_4 exhibited a maximum ZT of 0.39 at 623 K. However, this increase in ZT values was very small; a maximum ZT of 0.42 for $Cu_3Sb_{0.96}Al_{0.04}Se_4$ and 0.47 for $Cu_3Sb_{0.96}In_{0.04}Se_4$ occur at 623 K. The ZT values decreased as the Al and In doping content was increased further. Li et al. [13] achieved a ZT of 0.58 at 600 K for $Cu_3Sb_{0.97}Al_{0.03}Se_4$ prepared by the melting-quenching-annealing-SPS process, which was approximately 1.9 times higher than that of Cu_3SbSe_4. Zhang et al. [14] reported a ZT of 0.50 at 648 K for $Cu_3Sb_{0.997}In_{0.003}Se_4$ synthesized by the melting-quenching-annealing-HP method, which was a 47% improvement over the ZT value of Cu_3SbSe_4. In this study, doping with In was considered to be more effective than doping with Al for improving the thermoelectric performance of permingeatite. In addition, the solid-state synthesis process combining MA and HP is a simple and useful method that does not require subsequent heat treatment to produce homogeneous permingeatite compounds.

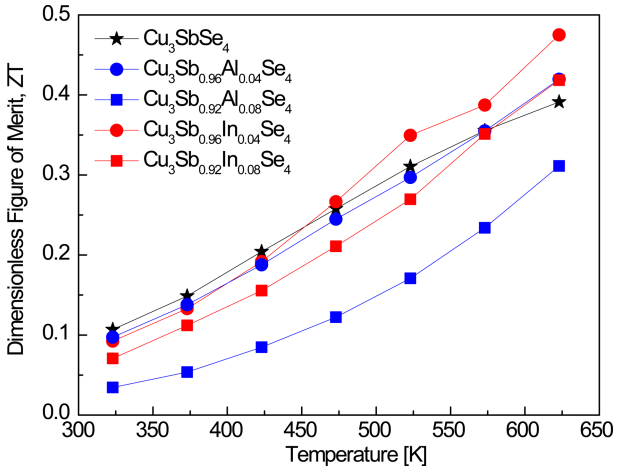

Fig. 9. Temperature dependence of the ZT values of $Cu_3Sb_{1-y}(Al/In)_ySe_4$.

4. CONCLUSIONS

$Cu_3Sb_{1-y}B^{III}{}_ySe_4$ (B^{III} = Al or In; $0 \le y \le 0.08$) permingeatite powders were synthesized by MA and sintering through HP. The phases, microstructures, charge-transport parameters, and thermoelectric properties were examined following the substitution of Al or In dopants at the Sb sites. In all specimens, a single permingeatite phase with a tetragonal structure was observed. Both undoped and Al/In-doped samples exhibited positive Seebeck and Hall coefficients, indicating p-type semiconductor characteristics. As the Al/In doping content increased, the carrier concentration increased, resulting in increased electrical conductivity and decreased Seebeck coefficient, compared to that of Cu_3SbSe_4. $Cu_3Sb_{0.96}Al_{0.04}Se_4$ achieved a maximum ZT value of 0.42 at 623 K and $Cu_3Sb_{0.96}In_{0.04}Se_4$ achieved a maximum ZT value of 0.47 at 623 K.

Acknowledgments

This study was supported by the Basic Science Research Capacity Enhancement Project (National Research Facilities and Equipment Center) through the Korea Basic Science

Institute funded by the Ministry of Education (Grant No. 2019R1A6C1010047).

REFERENCES

1. B. Wang, S. Zheng, Y. Chen, Q. Wang, Z. Li, Y. Wu, J. Li, Y. Mu, S. Xu, and J. Liang, *Mater. Today Energy* **19**, 100620 (2021).
2. A. Kumar, P. Dhama, and P. Banerji, *AIP Conf. Proc.* **1832**, 110050 (2016).
3. J. M. Li, H. W. Ming, B. L. Zhang, C. J. Song, L. Wang, H. X. Xin, J. Zhang, X. Y. Qin, and D. Li, *Mater. Chem. Front.* **5**, 324 (2021).
4. L. Min, Y. Xia, P. Ying, and J. Cui, *J. Appl. Phys.* **127**, 235104 (2020).
5. D. Zhang, J. Yang, Q. Jiang, Z. Zhou, X. Li, Y. Ren, J. Xin, A. Basit, X. He, W. Chu, and J. Hou, *J. Alloys Compd.* **724**, 597 (2017).
6. G. García, P. Palacios, A. Cabot, and P. Wahnón, *Inorg. Chem.* **57**, 7321 (2018).
7. J. M. Li, H. W. Ming, C. J. Song, L. Wang, H. X. Xin, Y. J. Gu, J. Zhang, X. Y. Qin, and D. Li, *Mater. Today Energy* **18**, 100491 (2020).
8. C. Yang, F. Huang, L. Wu, and K. Xu, *J. Phys. D: Appl. Phys.* **44**, 295404 (2011).
9. T. R. Wei, H. Wang, Z. M. Gibbs, C. F. Wu, G. J. Snyder, and J. F. Li, J. *Mater. Chem. A* **2**, 13527 (2014).
10. C. H. Chang, C. L. Chen, W. T. Chiu, and Y. Y. Chen, *Mater. Lett.* **186**, 227 (2017).
11. J. H. Pi, G. E. Lee, and I. H. Kim, *Korean J. Met. Mater.* **59**, 422 (2021).
12. D. Zhao, D. Wu, and L. Bo, *Energies* **10**, 1524 (2017).
13. Y. Li, X. Qin, D. Li, X. Li, Y. Liu, J. Zhang, C. Song, and H. Xin, *RSC Adv.* **5**, 31399 (2015).
14. D. Zhang, J. Yang, Q. Jiang, L. Fu, Y. Xiao, Y. Luo, and Z. Zhou, *Mater. Des.* **98**, 150 (2016).
15. R. D. Shannon, *Acta Crystallogr. A* **32**, 751 (1976).
16. A. L. Allred, *J. Inorg. Nucl. Chem.* **17**, 215 (1961).
17. V. B. Ghanwat, S. S. Mali, C. S. Bagade, R. M. Mane, C. K. Hong, and P. N. Bhosale, *Energy Technol.* **4**,1 (2016).
18. V. B. Ghanwat, S. S. Mali, C. S. Bagade, K. V. Khot, N. D. Desai, C. K. Hong, and P. N. Bhosale, *J. Mater. Sci.: Mater. Electron.* **29**, 8793 (2018).
19. H. Brooks, *Adv. Electron. Electron. Phys.* **7**, 85 (1955).
20. A. Suzumura, M. Watanabe, N. Nagasako, and R. Asahi, *J. Electron. Mater.* **43**, 2356 (2014).
21. Y. Yan, H. Wu, G. Wang, X. Lu, X. Zhou, *Energy Stor. Mater.* **13**, 127 (2018).
22. B. Wang, S. Zheng, Y. Chen, Y. Wu, J. Li, Z. Ji, Y. Mu, Z. Wei, Q. Liang, and J. Liang, *J. Phys. Chem.* **124**, 10336 (2020).
23. H. S. Kim, Z. M. Gibbs, Y. Tang, H. Wang, and G. J. Snyder, *APL Mater.* **3**, 041506 (2015).